

Transport Theory of Metallic B20 Helimagnets

Jian Kang^{1,*} and Jiadong Zang^{2,†}

¹*School of Physics and Astronomy, University of Minnesota, Minneapolis, MN 55455, USA*

²*Department of Physics and Astronomy, Johns Hopkins University, Baltimore, MD 21218, USA*

(Dated: December 24, 2014)

B20 compounds are a class of cubic helimagnets harboring nontrivial spin textures such as spin helices and skyrmions. It has been well understood that the Dzyaloshinskii-Moriya (DM) interaction is the origin of these textures, and the physics behind the DM interaction is the spin-orbital coupling (SOC). However the SOC shows its effect not only on the spins, but also on the electrons. In this paper, we will discuss effects of the SOC on the electron and spin transports in B20 compounds. An effective Hamiltonian is presented from symmetry analysis, and the spin-orbital coupling therein shows anomalous behaviors in anisotropic magnetoresistance (AMR) and helical resistance. New effects such as inverse spin-galvanic effect is proposed, and the origin of the DM interaction is discussed.

PACS numbers: 71.10.Ay, 72.10.Fk, 72.15.Gd, 75.10.Hk

I. INTRODUCTION

Symmetry is a central topic of modern physics and material science. Reduced symmetry has given rise to innumerable novel phenomena. For example, breaking of the translational symmetry leads to the emergence of lattices and crystals, which are the platforms of condensed matter studies. The highest symmetry of a lattice has the point group of O_h , where most of the ferromagnetic materials belong to. Surprises have been brought by further reducing this symmetry. B20 compound, with representatives of $\text{FeSi}^{1,2}$, MnSi^{3-5} , $\text{FeGe}^{6,7}$, and $\text{Cu}_2\text{SeO}_3^8$, is such an interesting class of materials. Although B20 compound has a cubic lattice, it has the lowest symmetry in this crystal system. Complicated distributions of atoms dramatically bring down the symmetry, where inversion, mirror, or four-fold rotational symmetries are absent. Abundant phenomena are emerging consequently, among which the most attractive one is the presence of nontrivial spin textures like helices and skyrmions.

Spin helix is a spatially modulated magnetic texture. It is present in magnetic materials with competing interactions. It has been observed in B20 family $\text{Fe}_{1-x}\text{Co}_x\text{Si}$ by real-space imaging⁹. In this case, the Dzyaloshinskii-Moriya (DM) interaction^{10,11}

$$H_{\text{DM}} = \mathbf{D} \cdot (\mathbf{S}_i \times \mathbf{S}_j) \quad (1)$$

between neighboring spins plays an important role. Broken inversion symmetry in B20 compounds is the physical origin of this interaction. Under an inversion operation about the center of the joint line, two neighboring spins are exchanged, and the DM interaction flips sign due to its cross product nature. In contrast, the Heisenberg exchange, $H_{\text{H}} = -J\mathbf{S}_i \cdot \mathbf{S}_j$ is unchanged under this operation, thus respects the inversion symmetry. The Heisenberg exchange tends to align neighboring spins, while the DM interaction tends to form an angle of $\pi/2$. As a result of the competition, a finite angle is expanded by these two spins, whose successive arrangement generates the spin

helix. Spin helix is not the only result of breaking inversion symmetry, but also the magnetic skyrmion^{3,12-14}, a topological spin texture. It is stabilized in B20 compounds at finite magnetic fields and temperatures.

In the light of nontrivial spin modulation in helix and promising spintronics applications of the skyrmion, a throughout understanding of the electron and spin transports in B20 compounds is an urgent subject. Longitudinal magnetoresistance measurements have been performed to map out the phase diagrams containing helical and skyrmion phases^{15,16}. On the other hand, due to the emergent electromagnetism^{17,18}, skyrmion phase can be precisely determined by the Hall measurements^{6,19-22}. A peculiar non-Fermi liquid behavior is also addressed in MnSi single crystals^{4,5}, which is intimately related to the topology of spin textures²³. However, a deep study of the spin transports in B20 compounds still lacks. Recently, an experiment on anisotropic magnetoresistance (AMR) is performed in bulk samples of $\text{Fe}_{1-x}\text{Co}_x\text{Si}^{24}$. It is surprisingly observed that compared to usual AMR in cobalt or other cubic ferromagnetic materials, the magnetoresistance shows two, instead of four, peaks. It shows that the system lacks of the four-fold rotational symmetry, which is compatible with the reduced symmetry in B20 compounds. However the microscopic origin waits to be revealed. In another experiment, the measurement on helical resistance shows an ultra-low resistance ratio of 1.35 with current parallel and perpendicular to the helix²⁵. It has predicted theoretically and well tested experimentally that this ratio should be larger than 3. This observation apparently violate this common concept.

These two experiments suggest a new mechanism involving nontrivial spin scatterings, and thus inevitably call for the important effects of the spin-orbital coupling (SOC) on the conduction electrons in B20 compounds. The SOC has already shows its power in the spin interactions in B20 compounds. It is well known that a non-vanishing DM interaction requires not only the inversion symmetry breaking, but also a large SOC¹¹. However effects of the SOC on conduction electrons have never been

discussed. In this paper, we will show that the SOC well explains the two experiments above, and provides several other proposals.

This paper is organized as follows. In the following section, an effective Hamiltonian is constructed, where both linear and cubic SOC terms are present. Section III shows that these SOC terms are the microscopic origin of the DM interactions in B20 compounds. In section IV and V, the linear SOC gives rise to inverse spin-galvanic effect and ultra-low ratio of helical resistance, respectively. In section VI, the importance of the cubic SOC is revealed, which provides the microscopic mechanism of the anomalous AMR effect.

II. EFFECTIVE HAMILTONIAN

In order to understand the transport behaviors of B20 compounds, the first priority is to construct the effective Hamiltonian of the conduction electrons. As we are interested in the long-range behaviors, only momenta around the Γ point will be relevant. The bands around other high symmetry points in the Brillouin zone might cross the Fermi energy, and contribute to the transports in some form. However, the qualitative behavior, especially the symmetries, will not change.

The importance of the SOC indicates that the conventional quadratic dispersion, $H(\mathbf{k}) = \hbar^2 \mathbf{k}^2 / 2m$, is not adequate in understanding the spin-related transports. Therefore, additional terms coupling spin and momentum is called for. To this end, we analyze the symmetry of the B20 compounds and employ the theory of invariants to construct the effective Hamiltonian²⁶.

In the international notation, the space group of B20 compounds is P_{213} , where 2 and 3 mean the two-fold and three-fold rotational symmetries respectively, while 1 indicates a fractal translation in the space group operation. No other symmetries are present. Around the Γ point, the fractal rotation does not change the space group irreducible representations²⁷, thus is not relevant, and the space group is isomorphic to its K-group, which is a group containing all the point group operations within the space group. Irreducible representations of the space group at Γ point is the same as that of the K-group. For P_{213} , the K-group is the $T23$ group, containing 12 elements; 1 identity, 3 C_2 rotations (π rotations about axis [100], [010], and [001], and 8 C_3 rotations (Clockwise rotations of $2\pi/3$ about directions $[\pm 1, \pm 1, \pm 1]$). Compared to the complete group operations in the O_h group, four-fold rotations, inversions, and mirror symmetries are absent.

Once spin is taken into account, a 2π rotation in the spin space reverses the sign, and should be treated as an additional group operation. One thus has to consider the double group of $T23$, whose irreducible representations and characters are listed in Tab. (I). Operations with bars are joint action of point group element and the 2π spin rotation.

First principle calculations on metallic B20 materials,

TABLE I: The character table for the double group of $T23$.

$T23$	E	\bar{E}	$4C_3$	$4\bar{C}_3$	$3C_2 + 3\bar{C}_2$	$4C_3^{-1}$	$4\bar{C}_3^{-1}$
Γ_1	1	1	1	1	1	1	1
Γ_2	1	1	w	w	1	w^2	w^2
Γ_3	1	1	w^2	w^2	1	w	w
Γ_4	3	3	0	0	-1	0	0
Γ_5	2	-2	1	-1	0	1	-1
Γ_6	2	-2	w	$-w$	0	w^2	$-w^2$
Γ_7	2	-2	w^2	$-w^2$	0	w	$-w$

such as MnSi and FeGe, show that the orbitals around the Fermi surface are mainly d-orbitals²⁸. Under spin-orbit coupling, these orbitals are split into $j = 5/2$ and $j = 3/2$ orbitals, which correspond to $D_{5/2}$ and $D_{3/2}$ irreducible representations of the rotation group respectively. The character of a rotation of angle α in D_j is given by

$$\chi = \frac{\sin((j + \frac{1}{2})\alpha)}{\sin(\frac{1}{2}\alpha)} \quad (2)$$

In the crystal field, these orbitals are further split into suborbitals, which corresponds to the decomposition in terms of $T23$'s irreducible representations;

$$D_{5/2} \downarrow T = \Gamma_5 \oplus \Gamma_6 \oplus \Gamma_7 \quad (3)$$

$$D_{3/2} \downarrow T = \Gamma_6 \oplus \Gamma_7 \quad (4)$$

In reality, all these suborbitals might be relevant around the Fermi surface. In addition, there are four magnetic atoms in each unit cell, leading to a total of 20 bands. In order to capture the key feature of these materials, we would like to keep the Hamiltonian in the minimal form. Only one band out of three representations $\Gamma_{5,6,7}$ will be considered. The resulting Hamiltonian will be two by two, the simplest Hamiltonian taking into account the SOC.

The model Hamiltonian H communicating the Hilbert spaces corresponding to irreducible representations α and β is in general

$$H(\mathbf{k}) = \sum_{l_1^\alpha=1}^{n_\alpha} \sum_{l_2^\beta=1}^{n_\beta} h(\mathbf{k}) |l_1^\alpha\rangle \langle l_2^\beta| \quad (5)$$

Here n_α and n_β are dimensions of these two representations respectively. In the current case, band mixing is neglected such that $\alpha = \beta$. l_1^α labels the basis in the irreducible representation α . The operator part $|l_1^\alpha\rangle \langle l_2^\beta|$ transforms as the product representation $\Gamma_\alpha^* \times \Gamma_\beta$, which can be decomposed as the direct sum of irreducible representations $\Gamma_\alpha^* \times \Gamma_\beta = \oplus_\gamma \Gamma_\gamma$. The basis $X_{l_3^\gamma}^\gamma$ of an irreducible representation Γ_γ contained in this product representation is the superposition of direct products $|l_1^\alpha\rangle \langle l_2^\beta|$ as $X_{l_3^\gamma}^\gamma = \sum_{l_1^\alpha=1}^{n_\alpha} \sum_{l_2^\beta=1}^{n_\beta} C_{l_1^\alpha l_2^\beta, l_3^\gamma}^{\alpha\beta, \gamma} |l_1^\alpha\rangle \langle l_2^\beta|$, where $C_{l_1^\alpha l_2^\beta, l_3^\gamma}^{\alpha\beta, \gamma}$ are

the Clebsh-Gordan coefficients²⁹. To keep the Hamiltonian invariant under group operations, $h(\mathbf{k})$ must be an irreducible tensor operator in the representation Γ_γ^* , such that $H(\mathbf{k})$ belongs to the trivial representation Γ_1 contained in the product representation $\Gamma_\gamma^* \times \Gamma_\gamma$. As a consequence, the invariant Hamiltonian is given by

$$H(\mathbf{k}) = \sum_{\gamma} a_{\gamma}^{\alpha\beta} \sum_1^{n_{\gamma}} h_{l_3^{\gamma}}^{\gamma}(\mathbf{k}) X_{l_3^{\gamma}}^{\gamma} \quad (6)$$

$$= \sum_{\gamma} a_{\gamma}^{\alpha\beta} \sum_1^{n_{\gamma}} h_{l_3^{\gamma}}^{\gamma}(\mathbf{k}) \left(\sum_{l_1^{\alpha}=1}^{n_{\alpha}} \sum_{l_2^{\beta}=1}^{n_{\beta}} C_{l_1^{\alpha} l_2^{\beta} l_3^{\gamma}}^{\alpha\beta, \gamma} |l_1^{\alpha}\rangle \langle l_2^{\beta}| \right) \quad (7)$$

where coefficients $a_{\gamma}^{\alpha\beta}$ are free parameters that cannot be dictated from the symmetry analysis.

For Γ_5 , $\Gamma_5^* \times \Gamma_5 = \Gamma_1 \oplus \Gamma_4$. However $X_1^{\Gamma_1}$ and all the three matrices $X_{1,2,3}^{\Gamma_4}$ are all trivial identity matrices. Therefore the effective can be reduced to be spinless, and spin-orbital coupling is absent. The corresponding Hamiltonian is therefore the simplest quadratic one $H(\mathbf{k}) = \hbar^2 \mathbf{k}^2 / 2m$, which does not bring anything new. New physics comes when we turn to Γ_6 or Γ_7 representations. As these two representations are complex conjugate to each other, the effective Hamiltonians are the same. In the following, we will take Γ_6 for example without loss of generality.

$$\Gamma_6^* \times \Gamma_6 = \Gamma_1 \oplus \Gamma_4 \quad (8)$$

$$\begin{aligned} X_1^{\Gamma_1} &= \begin{pmatrix} 1 & 0 \\ 0 & 1 \end{pmatrix}, X_1^{\Gamma_4} = \begin{pmatrix} 0 & -i/\sqrt{3} \\ -i/\sqrt{3} & 0 \end{pmatrix} \\ X_2^{\Gamma_4} &= \begin{pmatrix} 0 & 1/\sqrt{3} \\ -1/\sqrt{3} & 0 \end{pmatrix}, X_3^{\Gamma_4} = \begin{pmatrix} -i/\sqrt{3} & 0 \\ 0 & i/\sqrt{3} \end{pmatrix} \end{aligned} \quad (9)$$

It shows explicitly that $X_i^{\Gamma_4} = -i/\sqrt{3} \sigma_i$, where σ_i are three Pauli matrices. The overall factor $-i/\sqrt{3}$ can be absorbed into the factor $a_{\gamma}^{\alpha\beta}$ in Eq. (7). Now the remaining job is to construct the irreducible tensor operators $h_{l_3^{\gamma}}^{\gamma}(\mathbf{k})$. For Γ_1 , it is very simple that $h_1^{\Gamma_1}(\mathbf{k}) = \mathbf{k}^2 / 2m$. While for Γ_4 , two basis may apply. $h_i^{\Gamma_4}(\mathbf{k}) = (k_x, k_y, k_z)$, or $h_i^{\Gamma_4} = (k_x(k_y^2 - k_z^2), k_y(k_z^2 - k_x^2), k_z(k_x^2 - k_y^2))$, which are on the first and third orders in momentum \mathbf{k} respectively. Terms of second order in \mathbf{k} break the time reversal symmetry once coupled to the spin, thus can be neglected. As a consequence, the effective Hamiltonian for conduction electrons in B20 compounds is given by

$$\begin{aligned} H &= \frac{\mathbf{k}^2}{2m} + \alpha(k_x \sigma_x + k_y \sigma_y + k_z \sigma_z) \\ &+ \beta[k_x \sigma_x (k_y^2 - k_z^2) + k_y \sigma_y (k_z^2 - k_x^2) + k_z \sigma_z (k_x^2 - k_y^2)] \end{aligned} \quad (10)$$

This Hamiltonian can also be intuitively guessed from simple symmetry analysis. The presence of C_3 symmetry enforces the permutation symmetry in the Hamiltonian, while the C_2 symmetry rules out most of the combinations. It is worth emphasizing that the linear spin-orbital coupling $\mathbf{k} \cdot \boldsymbol{\sigma}$ is not adequate, as it is a full rotational symmetric term. C_4 symmetry is also respected by this term, but is apparently broken in $T23$ group. It is the cubic spin-orbital coupling, the last term in Eq. (10), that breaks C_4 . Therefore Eq. (10) is the minimal Hamiltonian that faithfully describes the symmetry of B20 compounds.

The cubic spin-orbital coupling is well known in III-V semiconductors induced by bulk inversion asymmetry (BIA)³⁰. The linear term $\mathbf{k} \cdot \boldsymbol{\sigma}$ is a new term. It will be discussed in the following that it captures most of the nontrivial physics in B20 compounds. As $\boldsymbol{\sigma}$ is a pseudo-vector, $\mathbf{k} \cdot \boldsymbol{\sigma}$ is a pseudo-scalar. This is thus a forbidden term in lattices with any inversion or mirror symmetries. That is why it is absent in the III-V semiconductors and most of the ferromagnetic materials. However, elements in the $T23$ point group are only pure rotations, so that $\mathbf{k} \cdot \boldsymbol{\sigma}$ is allowed, and contributes significantly to the long range behaviors.

III. ORIGIN OF SPIN INTERACTIONS

Real space images of B20 compounds have shown that the spin helix therein looks like a successive array of Bloch walls⁹, where magnetizations are rotating in a plane perpendicular to their propagation direction. In addition, the skyrmion has a double twist structure¹³. These features are well described by the DM interaction in the following shape

$$H_{DM} = D \hat{r}_{ij} \cdot (\mathbf{S}_i \times \mathbf{S}_j), \quad (11)$$

namely the DM vector \mathbf{D} in Eq. (1) should point from one spin to the other. Although it is compatible with the symmetry³¹, the microscopic origin still lacks. However, it can be understood by the SOC in our effective Hamiltonian as follows.

Quantitatively, we can employ the field approach to calculate the Ruderman-Kittel-Kasuya-Yosida (RKKY) interaction between two neighboring spins \mathbf{S}_1 and \mathbf{S}_2 ³²⁻³⁴. The electron's action is given by

$$\begin{aligned} S &= \sum_n \int d^3 \mathbf{k} \bar{\psi}(-\mathbf{k}, -i\omega_n) (-i\omega_n + \frac{\mathbf{k}^2}{2m} + \alpha \mathbf{k} \cdot \boldsymbol{\sigma}) \psi(\mathbf{k}, i\omega_n) \\ &+ \sum_{i=1}^2 \sum_n \int d^3 \mathbf{k} \bar{\psi}(-\mathbf{k} - \mathbf{q}, -i\omega_n) \mathbf{S}_i \cdot \boldsymbol{\sigma} e^{-i\mathbf{q} \cdot \mathbf{R}_i} \psi(\mathbf{k}, i\omega_n) \end{aligned} \quad (12)$$

where \mathbf{R}_i are the positions of two spins. The spin interaction can be derived by integrating out the electrons using the gradient expansion. Up to the second order,

the spin-spin interaction is given by

$$S_{\text{eff}} = -2 \sum_n \int d^3\mathbf{k} \text{Tr}[G(\mathbf{R}, i\omega_n) \mathbf{S}_1 \cdot \sigma G(-\mathbf{R}, i\omega_n) \mathbf{S}_2 \cdot \sigma] \quad (13)$$

where $\mathbf{R} = \mathbf{R}_1 - \mathbf{R}_2$, and $G(\mathbf{R}, i\omega_n)$ is the real-space Green's function defined as

$$\begin{aligned} G(\mathbf{R}, i\omega_n) &= \int d^3\mathbf{k} \frac{e^{-i\mathbf{k} \cdot \mathbf{R}}}{-i\omega_n + \frac{k^2}{2m} - \alpha \mathbf{k} \cdot \boldsymbol{\sigma}} \\ &= \int_0^\infty dk \int_0^\pi d\theta k^2 \sin \theta \\ &\quad \times \int_0^{2\pi} d\varphi \frac{i\omega_n - \frac{k^2}{2m} + \alpha \mathbf{k} \cdot \boldsymbol{\sigma}}{(-i\omega_n + \frac{k^2}{2m})^2 - \alpha^2 k^2} e^{-i\mathbf{k} \cdot \mathbf{R}} \end{aligned} \quad (14)$$

One can decompose the momentum \mathbf{k} into directions parallel with and perpendicular to \hat{R} as $\mathbf{k} = (\mathbf{k} \cdot \hat{R})\hat{R} + (\hat{R} \times \mathbf{k}) \times \hat{R} \equiv \mathbf{k}_\parallel + \mathbf{k}_\perp$. Apparently, because of $\mathbf{k}_\perp \cdot \mathbf{R} = 0$, $\exp(i\mathbf{k}_\perp \cdot \mathbf{R}) = 1$, and

$$\int_0^{2\pi} d\varphi \frac{\alpha \mathbf{k}_\perp \cdot \boldsymbol{\sigma}}{(-i\omega_n + \frac{k^2}{2m})^2 - \alpha^2 k^2} = 0. \quad (16)$$

The Only contribution comes from the coupling between \mathbf{k}_\parallel and Pauli matrices. Thus

$$\begin{aligned} G(\mathbf{R}, i\omega_n) &= \int_0^\infty dk \int_0^\pi d\theta k^2 \sin \theta \\ &\quad \times \int_0^{2\pi} d\varphi \frac{i\omega_n - \frac{k^2}{2m} + \alpha \mathbf{k}_\parallel \cdot \boldsymbol{\sigma}}{(-i\omega_n + \frac{k^2}{2m})^2 - \alpha^2 k^2} e^{-i\mathbf{k}_\parallel \cdot \mathbf{R}} \\ &= 2\pi \int_0^\infty dk \int_0^\pi d\theta k^2 \sin \theta \\ &\quad \times \frac{i\omega_n - \frac{k^2}{2m} + \alpha k \cos \theta \hat{R} \cdot \boldsymbol{\sigma}}{(-i\omega_n + \frac{k^2}{2m})^2 - \alpha^2 k^2} e^{-ikR \cos \theta} \\ &\equiv G_0(R) + G_1(R) \mathbf{R} \cdot \boldsymbol{\sigma} \end{aligned} \quad (17)$$

where

$$G_0(R) = 2\pi \int_0^\infty dk \int_0^\pi d\theta \frac{k^2 \sin \theta (i\omega_n - \frac{k^2}{2m})}{(-i\omega_n + \frac{k^2}{2m})^2 - \alpha^2 k^2} e^{-ikR \cos \theta} \quad (18)$$

and

$$G_1(R) = \frac{2\pi}{R} \int_0^\infty dk \int_0^\pi d\theta \frac{\alpha k^3 \sin \theta \cos \theta}{(-i\omega_n + \frac{k^2}{2m})^2 - \alpha^2 k^2} e^{-ikR \cos \theta} \quad (19)$$

One can easily get these Green's functions by evaluating contour integrals. The real part of the poles of k gives rise to the Friedel oscillations.

Consequently, the effective RKKY Hamiltonian is given by

$$H^{\text{RKKY}} = -\frac{2}{\beta} \sum_n [(G_0^2 + G_1^2) \mathbf{S}_1 \cdot \mathbf{S}_2 + 2G_0 G_1 \mathbf{R} \cdot (\mathbf{S}_1 \times \mathbf{S}_2)] \quad (20)$$

The first term in the Heisenberg exchange, while the second term is the DM interaction. Compared to Eq. (1), the DM vector \mathbf{D} is along $\mathbf{R} = \mathbf{R}_1 - \mathbf{R}_2$, which is consistent with Eq. (11) for B20 compounds. One can easily show that even the cubic spin orbital coupling in Eq. (10) is included, the direction of DM vector is still unchanged. Thus the SOC in Eq. (10) gives rise to the right DM interactions in B20, and therefore the right physical origin. In the following two sections, we will discuss the effects of these two SOC terms in the collective transports.

The physical picture behind this calculation is the following. By the linear spin-orbital coupling $\alpha \mathbf{k} \cdot \boldsymbol{\sigma}$, the conduction electron feels effectively a magnetic field $-\alpha \mathbf{k} \sim -\alpha m \mathbf{v} / \hbar$. Therefore once it hops from one site to the other, its spin must precess about the effective magnetic field along the joint line between these two sites. The coupling between conduction electron and local magnetic moments thus reduces the energy once the moments at these two sites precess in the same way. The direction of the DM vector \mathbf{D} is thus parallel with the effective field, which point one spin to the other.

In reality, the interaction between the neighboring spins might have various origins besides the RKKY mechanism. However the physical picture of spin precession persists in any mechanism. Therefore the DM interaction always has the desired form once the spin orbital coupling, Eq. (10), is present.

Interesting consequence follows when an ultra-thin film of B20 compound is grown along [001] direction, and an electric field is applied perpendicular to the film. The intrinsic linear SOC gives $H = \alpha(k_x \sigma_x + k_y \sigma_y)$, while the additional Rashba SOC induced by the electric field is $H = \alpha_R(k_x \sigma_y - k_y \sigma_x)$. Still the intrinsic SOC gives DM interactions with DM vector pointing from one spin to the neighbor on the film. However the Rashba SOC contributes a DM vector perpendicular to the intrinsic one. In B20 compounds the spin helix looks like a successive array of Bloch domain walls, where the spins are rotating in a plane perpendicular to the propagation direction. However in the large α_R limit, the resulting spin helix is a successive array of Neel walls, where the spins are coplanar to the propagation direction. Therefore by increasing the electric field, one can expect a gradual deformation of the spin helix. Similarly, the skyrmion will deform to that generated by interfacial DM interactions³⁵. These deformations can be observed by Lorentz TEM images.

IV. INVERSE SPIN-GALVANIC EFFECT

There have been extensive discussions on the interaction between the conduction electrons and local magnetic moments \mathbf{M} in metallic magnets. These two are directly coupled to each other via the Hund's rule coupling $H = -J_H \mathbf{M} \cdot \boldsymbol{\sigma}$, where $\boldsymbol{\sigma}$ is the spin of the conduction electron. In the adiabatic limit, $J_H \rightarrow \infty$, electron spins are parallel with the local moments. Algebraically, one can perform an $SU(2)$ transformation U

such that $U^\dagger \mathbf{M} \cdot \boldsymbol{\sigma} U = \sigma_z$. In the adiabatic limit, only the up spin, namely the upper-left part of the transformed Hamiltonian, is relevant. In case moments are spatially non-uniform, the same U rotation transforms the kinetic energy $\mathbf{k}^2/2m$ to $(\mathbf{k} - e\mathbf{A})^2/2m$, where $SU(2)$ gauge field $e\mathbf{A}_\mu = -iU^\dagger \partial_\mu U^{36}$, whose upper-left part \mathbf{A} is the real-space emergent electromagnetic field¹⁷. The minimal coupling between \mathbf{A} and the electric current \mathbf{j} results in the current driven domain wall or the skyrmion motions^{17,37}.

The scenario above is no longer valid in the presence of the SOC. Due to the non-commutative nature of the Pauli matrices, the conduction electrons feel more than the emergent electromagnetic field \mathbf{A} , and additional coupling to the electric current needs to be included. Careful analysis is required in the current case.

One can similarly perform an $SU(2)$ gauge transformation U to the Hamiltonian

$$H = \frac{1}{2m} \mathbf{k}^2 + \alpha \mathbf{k} \cdot \boldsymbol{\sigma} - J_H M(r) \cdot \boldsymbol{\sigma} \quad (21)$$

so that $U^\dagger M(r) \cdot \boldsymbol{\sigma} U = m\sigma_z$. The first term again gives rise to $U^\dagger (\mathbf{k}^2/2m) U = (\mathbf{k} - e\mathbf{A})^2/2m$, with $e\mathbf{A}_\mu = -iU^\dagger \partial_\mu U$, while the second one is transformed as

$$U^\dagger \mathbf{k} \cdot \boldsymbol{\sigma} U = U^\dagger \sigma_\mu U (k_\mu - e\mathbf{A}_\mu) \quad (22)$$

In the adiabatic limit, we take the upper-left ($\uparrow\uparrow$) part of the transformed Hamiltonian, so that

$$H = \frac{1}{2m} (\mathbf{k} - e\mathbf{A})^2 + \alpha (\mathbf{f} \cdot \mathbf{k} - g) - J_H m \quad (23)$$

where $f_\mu = [U^\dagger \sigma_\mu U]_{\uparrow\uparrow}$, and $g = [\mu U^\dagger \sigma_\mu U e\mathbf{A}_\mu]_{\uparrow\uparrow}$. As $\dot{\mathbf{x}} = \frac{\partial H}{\partial \mathbf{k}} = \frac{1}{m} (\mathbf{k} - e\mathbf{A}) + \alpha \mathbf{f}$, the Lagrangian is given by

$$\begin{aligned} L &= \mathbf{k} \cdot \dot{\mathbf{x}} - H \\ &= \frac{1}{2} m \dot{\mathbf{x}}^2 + e\mathbf{A} \cdot (\dot{\mathbf{x}} - \alpha \mathbf{f}) - m\alpha \mathbf{f} \cdot \dot{\mathbf{x}} + \frac{1}{2} m\alpha^2 \mathbf{f}^2 + \alpha g \end{aligned} \quad (24)$$

The electric current $\mathbf{j} = e\dot{\mathbf{x}}$ thus minimal couples to $(\mathbf{A} - \frac{m\alpha}{e}\mathbf{f})$, instead of \mathbf{A} in the absence of the SOC. For local magnetizations $\hat{m} = (\sin\theta \cos\phi, \sin\theta \sin\phi, \cos\theta)$, let $U = u_0 + i\mathbf{u} \cdot \boldsymbol{\sigma}$. Up to a gauge, we get $u_0 = \frac{1}{2\sin(\theta/2)}$, $\mathbf{u} = \frac{1}{2\sin(\theta/2)} \hat{z} \times \hat{m}$, and consequently $\mathbf{f} = \hat{m}$. The effective coupling between magnetization and the current is thus given by

$$L_c = \frac{1}{e} \mathbf{j} \cdot (e\mathbf{A} - \alpha \mathbf{m}) \quad (25)$$

By varying the total action, the magnetization dynamics obeys the following equation of motion;

$$\dot{\mathbf{m}} + \frac{1}{e} \mathbf{j} \cdot \nabla \mathbf{m} - \frac{\alpha}{e} \mathbf{m} \times \mathbf{j} + \mathbf{m} \times \mathbf{H}_{eff} = 0 \quad (26)$$

The third term is the contribution from SOC. It shows explicitly that via SOC, an electric current \mathbf{j} serves as

an effective planar field acting on the magnetizations, manifesting the inverse spin-galvanic effect.

The physics of the inverse spin-galvanic effect is very simple. Under a steady electric current, the Fermi surface acquires a shift along the current direction, and ends up with a nonvanishing average momentum $\langle \mathbf{k} \rangle$ in the same direction. The SOC $\alpha \mathbf{k} \cdot \boldsymbol{\sigma}$ thus reduces energy when the spin $\langle \boldsymbol{\sigma} \rangle$ is antiparallel with \mathbf{j} . This average spin provide a spin transfer torque on the local magnetizations, which is therefore analogous to a effective magnetic field along $-\mathbf{j}$.

Although the effective field along the current will not change routine observables such as the topological Hall effect¹⁹, a physical consequence of this inverse spin-galvanic effect is the current induced helix reorientations in the helimagnet. It has been shown that the hysteresis under low field is vanishingly small in B20 compounds³⁸. The orientation of the spin helix is completely determined by the direction of external magnetic field. Here we propose that one can use an electric current, instead of magnetic fields, to orient the spin helix. The helix would propagate in parallel with the current, which can be experimentally confirmed by neutron scattering. This effect also applies in B20 thin film, where the Lorentz TEM would be a proper way to detect.

V. HELICAL RESISTANCE

The SOC has various consequences in the magnetoresistances. Under a low external magnetic field, the ground state of B20 is the helical state, assembling a successive arrays of magnetic domains. The domain wall resistance originated from collective spin scattering has been extensively studied both experimentally and theoretically in the context of conventional ferromagnets. SOC would apparently alter the the spin scattering, and leads to unconventional helical resistance in B20 compounds.

We consider the Hamiltonian in Eq. (10) while including of the Zeeman term $\boldsymbol{\sigma} \cdot \mathbf{h}$.

$$\begin{aligned} H &= \frac{k^2}{2m} - \mu + \mathbf{h} \cdot \boldsymbol{\sigma} + \alpha \mathbf{k} \cdot \boldsymbol{\sigma} + \beta \left(k_x (k_y^2 - k_z^2) \sigma_x \right. \\ &\quad \left. + k_y (k_z^2 - k_x^2) \sigma_y + k_z (k_x^2 - k_y^2) \sigma_z \right) \end{aligned} \quad (27)$$

$$U(\mathbf{r}) = \frac{1}{N} \sum_i (v I_{2 \times 2} - j \mathbf{h} \cdot \boldsymbol{\sigma}) \delta_{\mathbf{r}, \mathbf{R}_i} \quad (28)$$

Here, \mathbf{h} is the local magnetization. It rotates in yz plane perpendicular to x , the propagation direction. U is the impurity potential, including both the scalar potential v and spin-dependent potential $-j \mathbf{h} \cdot \boldsymbol{\sigma}$ ³⁹. In the domain wall, the direction of magnetization is nonuniform. Under the assumption of slowly varying spin configuration (the helix period $d \gg 1/k_f$), one can perform an $SU(2)$ gauge transformation R to the Hamiltonian so that the spin in the domain wall points along \hat{e}_z direction. R is

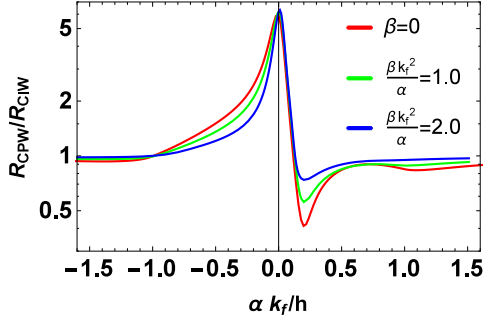


FIG. 1: The resistance ratio R_{CPW}/R_{CIW} vs the spin orbital coupling. In the plot, $\pi k_f/(mdh) = 0.2$, $j\hbar/v = 1.06$. Different curves are for different cubic SOC terms. It is clear that the ratio approaches to the one when the SOC is much larger than the Zeeman energy \hbar .

set to be

$$R = \exp(-i\theta(x)\sigma_x) \quad (29)$$

with $\theta(x) = 2\pi x/d$ where d is the helix period. By this rotation,

$$\begin{aligned} R^{-1}(\sigma \cdot \hat{h})R &= \sigma_z \\ R^{-1}\frac{\hbar^2\nabla^2}{2m}R &= \frac{\hbar^2\nabla^2}{2m} - i\frac{\hbar^2}{2m}\sigma_x(\partial_x\theta)\partial_x \\ &= \frac{\hbar^2\nabla^2}{2m} - i\frac{\pi\hbar^2}{md}\sigma_x\partial_x \\ R^{-1}\sigma_x\partial_xR &= -i\frac{\pi}{d} + \sigma_x\partial_x \\ R^{-1}\sigma_y\partial_yR &= (\cos\theta\sigma_y - \sin\theta\sigma_z)\partial_y \\ R^{-1}\sigma_z\partial_zR &= (\cos\theta\sigma_z + \sin\theta\sigma_y)\partial_z \end{aligned}$$

The cubic SOC terms are transformed in a more complicated way. However, under the large helix period approximation, $d \gg 1/k_f$ with k_f the Fermi wavevector, it can be simplified as

$$\begin{aligned} R^{-1}\sigma_x k_x(k_y^2 - k_z^2)R &\approx \sigma_x k_x(k_y^2 - k_z^2) \\ R^{-1}\sigma_y k_y(k_z^2 - k_x^2)R &\approx (\sigma_y \cos\theta - \sigma_z \sin\theta)k_y(k_z^2 - k_x^2) \\ R^{-1}\sigma_y k_z(k_x^2 - k_y^2)R &\approx (\sigma_z \cos\theta + \sigma_y \sin\theta)k_z(k_x^2 - k_y^2) \end{aligned}$$

To calculate the helical conductivity, we solve the Boltzmann equation by a perturbation method. The deviation of electron distribution function from the equilibrium one $f_1 = f - f_0$ is expanded in terms of the spherical harmonic functions $Y_l^m(\theta, \phi)$ up to $l = 5$. The details of the calculation can be found in the appendix.

Fig 1 shows the ratio between the longitudinal resistivities with current perpendicular to the domain wall (CPW) and current in the domain wall (CIW). It is found that the ratio is strongly suppressed by the presence of the SOC. In addition, the presence of cubic SOC terms only quantitatively change the ratio.

The minimum of the ratio is reached when

$$\alpha = \frac{\pi}{md}. \quad (30)$$

To understand this minimum, we consider the Hamiltonian with the linear SOC coupling only, ie. $\beta = 0$. After the local $SU(2)$ gauge transformation, the Hamiltonian becomes

$$H = H_0 + V + \text{const.} \quad (31)$$

$$H_0 = \frac{p^2}{2m} - \hbar\sigma_z$$

$$V = \left(\alpha - \frac{\pi}{md}\right)\sigma_x p_x + \alpha\sigma_y(p_y \cos\theta + p_z \sin\theta) + \alpha\sigma_z(p_z \cos\theta - p_y \sin\theta) \quad (32)$$

$$\text{const} = \frac{\pi^2}{8md^2} - \frac{\alpha\pi}{2d}.$$

To simplify the notation, we define $\gamma = \alpha - \frac{\pi}{md}$. If SOC terms αk_f , βk_f^3 are much smaller than the Zeeman energy, the eigenstate of the Hamiltonian can be solved based on perturbation. In addition, we assume that the impurity scattering is strongly spin-dependent, ie. $v \approx j\hbar$. In this case, the conductivity is dominated by the outer Fermi surface, with its intraband impurity scattering given by

$$|M_{k \rightarrow k'}^{++}|^2 \approx (v + j\hbar)^2 \left[\frac{\gamma^2 k_x k'_x + \frac{\alpha^2}{2}(k_y k'_y + k_z k'_z)}{4\hbar^2} \right]^2 \quad (33)$$

Here, $+$ is for outer Fermi surface. When α vanishes, it is clear that scattering is larger at larger k_x and k'_x . The resistivity comes from the fermions with larger momentum along the direction of the current. Therefore, $\rho_x \gg \rho_{y/z}$, and thus the ratio R_{CPW}/R_{CIW} reaches its maximum. When $\gamma = 0$ ($\alpha = \pi/(md)$), the scattering rate is larger for larger $k_{y/z}$ and $k'_{y/z}$. Therefore, $\rho_{y/z} \gg \rho_x$, and the ratio R_{CPW}/R_{CIW} reaches the minimum. More detailed information can be found in the appendix.

VI. ANOMALOUS ANISOTROPIC MAGNETORESISTANCE

In previous sections, we have mainly focused on the effects of the linear SOC in Eq. (10). The cubic SOC only slightly modifies these effects. The cubic term fails to bring any qualitative change in these experiments. However from the symmetry's point of view, only the cubic SOC breaks the C_4 rotation, and it must give rise to anisotropic behaviors of the magnetoresistance. To this end, we study the case when external magnetic field is sufficiently large to polarize all magnetic moments along its direction, and calculate the magnetoresistances. It is well known that for most of the cubic ferromagnets such as Ni, the anisotropic magnetoresistance (AMR) shows four fold symmetry when the magnetic field rotates in the plane perpendicular to the current. However it has already been reported that in B20 compounds such as $\text{Fe}_{1-x}\text{Co}_x\text{Si}^{24}$, the AMR shows anomalous behavior that only a two fold symmetry is respected. In this section, we will show how the cubic SOC leads to this observation.

The same model as the previous section is employed. The Hamiltonian and the impurity potential is in the same form as Eq. (27) and Eq. (28). The conductivity $\sigma_{zz}(\mathbf{h})$ is calculated while varying the magnetization \mathbf{h} in the x-y plane. Most of the ferromagnetic materials have high symmetry and respect C_4 symmetry. Thus $\sigma_{zz}(h\hat{e}_x) = \sigma_{zz}(h\hat{e}_y)$ in these cases. However due to the C_4 breaking in B20 compounds, the anomalous AMR is expected where the ratio between two conductivities $\sigma_{zz}(h\hat{e}_x)$ and $\sigma_{zz}(h\hat{e}_y)$ deviates from 1.

Before calculation, let's explore the symmetries of the Hamiltonian in Eq. (27). It is found that

$$H(\alpha, \beta, h\hat{e}_y) = SH(\alpha, -\beta, h\hat{e}_x)S^{-1} \quad (34)$$

Here S is the operator which rotates the system along z axis by $\pi/2$. Therefore,

$$\sigma_{zz}(\alpha, \beta, h\hat{e}_x) = \sigma_{zz}(\alpha, -\beta, h\hat{e}_y) \quad (35)$$

In addition, the conductivity is invariant under the space inversion symmetry P ,

$$\begin{aligned} H(-\alpha, -\beta, \mathbf{h}) &= PH(\alpha, \beta, \mathbf{h})P^{-1} \\ \Rightarrow \sigma_{zz}(\alpha, \beta, \mathbf{h}) &= \sigma_{zz}(-\alpha, -\beta, \mathbf{h}) \end{aligned} \quad (36)$$

Combined with Eq. (35), it is concluded that

$$\sigma_{zz}(\alpha, \beta, h\hat{e}_x) = \sigma_{zz}(\alpha, -\beta, h\hat{e}_y) = \sigma_{zz}(-\alpha, \beta, h\hat{e}_y) \quad (37)$$

Solely by symmetry argument, it is found that the anomalous AMR, defined as $\sigma_{zz}(h\hat{e}_x)/\sigma_{zz}(h\hat{e}_y) - 1$, vanishes if either of two spin orbital couplings, α and β , vanishes. Similarly, we have $\sigma_{zz}(\alpha, \beta, h\hat{e}_h) = \sigma_{zz}(\alpha, \beta, -h\hat{e}_h)$.

In this section, the conductivity is calculated in the same way as the previous section. The Boltzmann equation is solved by perturbation method. The deviation of the electron distribution function is expanded by spherical harmonic functions up to $l = 5$. The anisotropy comes from two different sources. (i) the Fermi surface is anisotropic since the Hamiltonian in Eq. (27) breaks C_4 symmetry. (ii) the eigenstate on the Fermi surface is anisotropic, and thus leads to the anisotropic impurity scattering by the spin-dependent potential in Eq. (28).

The energy of the Hamiltonian in Eq. (27) is given by

$$\begin{aligned} \varepsilon_F &= \frac{\hbar^2 k_F^2}{2m} \pm \left(h_z^2 + \alpha^2(k_x^2 + k_y^2 + k_z^2) \right. \\ &\quad \left. + \beta^2[k_x^2(k_y^2 - k_z^2) + k_y^2(k_z^2 - k_x^2) + k_z^2(k_x^2 - k_y^2)] \right. \\ &\quad \left. + 2h_z k_z[\alpha + \beta(k_x^2 - k_y^2)] \right)^{1/2} \end{aligned} \quad (38)$$

The system contains two Fermi surfaces (FSs) since the Kramers degeneracy is lifted. All terms in Eq. (38) respect the symmetry exchanging the indices x and y except the last term in square root. It shows explicitly that the Fermi surface asymmetry is possible only when the magnetization is nonzero.

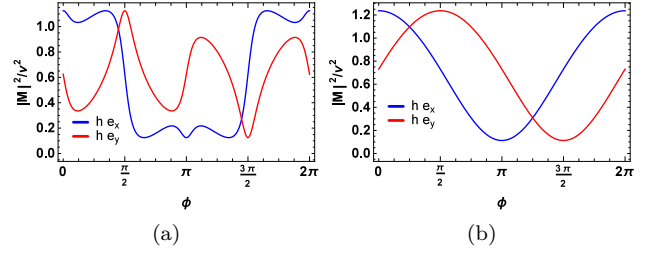


FIG. 2: The intraband impurity scattering amplitude from $(0, 0, k_f)$ to $(k_f \cos \phi, k_f \sin \phi, 0)$ on the outer Fermi surface. Red and blue curves are the scattering magnitude as a function of ϕ when the magnetization field points along \hat{y} and \hat{x} respectively, respectively. (a) The Zeeman energy is artificially turned off, while the impurity spin dependent is kept to be nonzero with $v/(jh) = 2.0$ and $\beta k_f^2/\alpha = 1.5$. The C_4 symmetry is broken in the impurity scattering amplitude. (b) $\beta = 0$. Both the Zeeman energy and the impurity spin-dependent potential are nonzero with $h/(ak_f) = 0.1$, and $v/(jh) = 2.0$. It is clear that C_4 symmetry recovers for $\beta = 0$.

However, the impurity scattering asymmetry is present as long as α and β are non-zero. Fig. 2 shows the intraband scattering magnitude $|M|^2$ from $(0, 0, k_f)$ to $(k_f \cos \phi, k_f \sin \phi, 0)$ on the outer Fermi surface. Red and blue curves are $|M|^2$ as a function of ϕ when the impurity magnetization points along \hat{y} and \hat{x} , respectively. If the C_4 symmetry is kept, the blue curve should be the same as the red one after a translation of $\pi/2$, which is apparently not the truth. It is noticeable that even when Zeeman field vanishes, the impurity scattering still breaks the C_4 symmetry, although the shape of Fermi surface is still C_4 symmetric. Of course in reality, both the Zeeman term and spin-dependant scattering coexist.

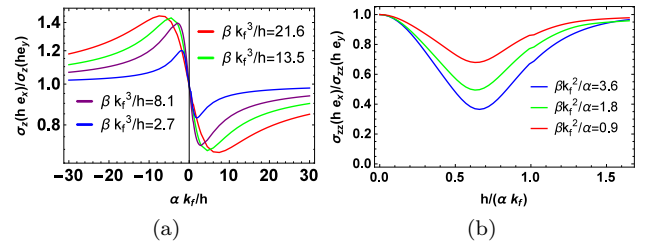


FIG. 3: The ratio $\sigma_z(h\hat{e}_x)/\sigma_z(h\hat{e}_y)$ vs SOC couplings and the magnetization field. (a) The ratio as a function of SOC with $v/(jh) = 2.0$. It becomes one when $\alpha = 0$ or $\beta k_f^2/\alpha \rightarrow 0$. This agrees with our conclusion in Eq.(37) by symmetry argument. (b) The ratio vs Zeeman energy h with $j = 1.0$. The anomalous AMR vanishes when $h = 0$ or $h \rightarrow \infty$.

Fig 3(a) shows the ratio $\sigma_{zz}(h\hat{e}_x)/\sigma_{zz}(h\hat{e}_y)$ as a function of the SOC. The ratio is smaller than 1 when α and β have the same sign, and larger than 1 when two SOC's have different signs. This is consistent with the conclusion Eq. (37) derived by symmetry arguments. In addition, it is found that the anomalous AMR vanishes

when either $\alpha = 0$ or $\alpha \rightarrow \infty$. The latter implies that the anomalous AMR vanishes when $\beta \rightarrow 0$. This result agrees with our physical picture based on the Fermi surface topology. C_4 symmetry is restored on the Fermi surface when $\beta \rightarrow 0$.

Fig 3(b) shows the anomalous AMR as a function of the magnetization field h . When h vanishes, not only the Zeeman energy vanishes, but also the impurity potential becomes spin-independent. Therefore, the impurity scattering becomes C_4 symmetric, as well as the Fermi surface. In this case, anomalous AMR vanishes. Our calculations agree well with the experimental results²⁴. When the temperature is raised above the Curie temperature, the anomalous AMR vanishes. This corresponds to the case with vanishing magnetization \mathbf{h} . In another limit when $h \rightarrow \infty$, the spin on the Fermi surface is fixed by the Zeeman energy. In this situation, the impurity scattering and Fermi surface become isotropic, and therefore the anomalous AMR vanishes.

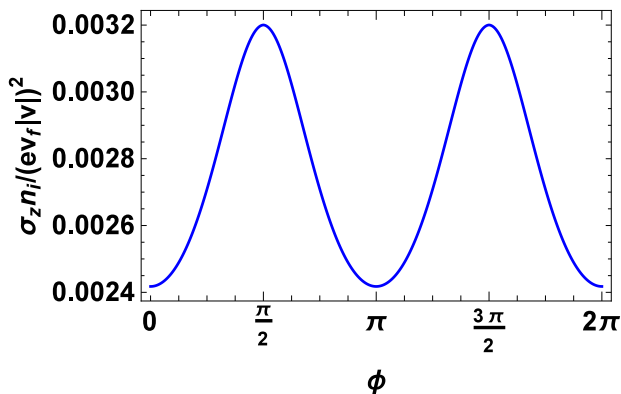


FIG. 4: Conductivity vs direction of in-plane magnetization field. In the plot, $\alpha k_f/h = 3.0$, $\beta k_f^3/h = 5.4$, and $v/(jh) = 2.0$. n_i is the impurity density.

Fig 4 shows the variation of the conductivity σ_{zz} as the direction of in-plane magnetization field changes. Note that σ_{zz} reaches its minimum(maximum) when the field points along $x(y)$ direction. In our calculation, this comes from that assumption that two SOC couplings have the same sign. If α and β have different signs, the minimum(maximum) is reached when \mathbf{h} is along $y(x)$ axis. This result reproduces the experimental observations in²⁴.

VII. CONCLUSION

In conclusion, the spin-orbital coupling is the fountain of various interesting phenomena in B20 compounds. It not only provides the antisymmetric spin interactions, but also dramatically change behaviors of the electron transport. The effective Hamiltonian constructed in this work captures the main effects of the SOC in conduction electrons. Despite its simple form, the emergent new physics is closely associated with several experiments. It also calls for bunch of future works to study the spin transports related to this Hamiltonian. First principle calculations are also encouraged to determine the strength of the SOC.

We are grateful for fruitful discussions with C. L. Chien, N. Nagaosa, S. X. Huang, C. X. Liu, O. Tchernyshyov, R. M. Fernandes, V. Galitski, and R. B. Tao. JK was supported by the Office of Basic Energy Sciences U.S. Department of Energy under awards numbers DE-SC0012336. JZ was supported by the TIPAC, by the U.S. Department of Energy under Award DEFG02-08ER46544, and by the National Science Foundation under Grant No. ECCS-1408168.

* Electronic address: jkang@umn.edu

† Electronic address: jiadongzang@gmail.com

¹ Z. Schlesinger, Z. Fisk, H.-T. Zhang, M. B. Maple, J. DiTusa, and G. Aeppli, *Physical Review Letters* **71**, 1748 (1993), URL <http://link.aps.org/doi/10.1103/PhysRevLett.71.1748>.

² J. F. DiTusa, K. Friemelt, E. Bucher, G. Aeppli, and A. P. Ramirez, *Physical Review Letters* **78**, 2831 (1997), URL <http://link.aps.org/doi/10.1103/PhysRevLett.78.2831>.

³ S. Mühlbauer, B. Binz, F. Jonietz, C. Pfleiderer, A. Rosch, A. Neubauer, R. Georgii, and P. Böni, *Science* **323**, 915 (2009), ISSN 0036-8075, 1095-9203, URL <http://www.sciencemag.org/content/323/5916/915>.

⁴ C. Pfleiderer, D. Reznik, L. Pintschovius, H. v. Löhneysen, M. Garst, and A. Rosch, *Nature* **427**, 227 (2004), ISSN 0028-0836, URL <http://www.nature.com/nature/journal/v427/n6971/abs/nature02232.html>.

⁵ R. Ritz, M. Halder, M. Wagner, C. Franz, A. Bauer, and C. Pfleiderer, *Nature* **497**, 231 (2013), ISSN 0028-0836, URL <http://www.nature.com/nature/journal/v497/n7448/abs/nature12048.html>.

⁶ S. X. Huang and C. L. Chien, *Phys. Rev. Lett.* **108**, 267201 (2012), URL <http://link.aps.org/doi/10.1103/PhysRevLett.108.267201>.

⁷ X. Z. Yu, N. K. anazawa, Y. Onose, K. Kimoto, W. Z. Zhang, S. Ishiwata, Y. Matsui, and Y. Tokura, *Nat Mater* **10**, 106 (2011), URL <http://www.nature.com/nmat/journal/v10/n2/abs/nmat2916.html>.

⁸ S. Seki, X. Z. Yu, S. Ishiwata, and Y. Tokura, *Science* **336**, 198 (2012), URL <http://www.sciencemag.org/content/336/6078/198.full.html>.

⁹ M. Uchida, Y. Onose, Y. Matsui, and Y. Tokura, *Science* **311**, 359 (2006), ISSN 0036-8075, 1095-9203, URL <http://www.sciencemag.org/content/311/5759/359>.

- ¹⁰ I. Dzyaloshinsky, *Journal of Physics and Chemistry of Solids* **4**, 241 (1958), ISSN 0022-3697, URL <http://www.sciencedirect.com/science/article/pii/0022369758900763>.
- ¹¹ T. Moriya, *Physical Review* **120**, 91 (1960), URL <http://link.aps.org/doi/10.1103/PhysRev.120.91>.
- ¹² T. H. R. Skyrme, *Proceedings of the Royal Society of London. Series A. Mathematical and Physical Sciences* **260**, 127 (1961), ISSN 1364-5021, 1471-2946, URL <http://rspa.royalsocietypublishing.org/content/260/1308/127>.
- ¹³ X. Z. Yu, Y. Onose, N. Kanazawa, J. H. Park, J. H. Han, Y. Matsui, N. Nagaosa, and Y. Tokura, *Nature* **465**, 901 (2010), ISSN 0028-0836, URL <http://www.nature.com/nature/journal/v465/n7300/full/nature09121>.
- ¹⁴ U. K. Rö\ssler, A. N. Bogdanov, and C. Pfleiderer, *Nature* **442**, 797 (2006), ISSN 0028-0836, URL <http://www.nature.com/nature/journal/v442/n7104/full/nature05056>.
- ¹⁵ K. Kadowaki, K. Okuda, and M. Date, *Journal of the Physical Society of Japan* **51**, 2433 (1982), ISSN 0031-9015, URL <http://journals.jps.jp/doi/abs/10.1143/JPSJ.51.2433>.
- ¹⁶ H. Du, J. P. DeGrave, F. Xue, D. Liang, W. Ning, J. Yang, M. Tian, Y. Zhang, and S. Jin, *Nano Letters* **14**, 2026 (2014), ISSN 1530-6984, URL <http://dx.doi.org/10.1021/nl5001899>.
- ¹⁷ J. Zang, M. Mostovoy, J. H. Han, and N. Nagaosa, *Physical Review Letters* **107**, 136804 (2011), URL <http://link.aps.org/doi/10.1103/PhysRevLett.107.136804>.
- ¹⁸ T. Schulz, R. Ritz, A. Bauer, M. Halder, M. Wagner, C. Franz, C. Pfleiderer, K. Everschor, M. Garst, and A. Rosch, *Nature Physics* **8**, 301 (2012), ISSN 1745-2473, URL <http://www.nature.com/nphys/journal/v8/n4/full/nphys2231>.
- ¹⁹ A. Neubauer, C. Pfleiderer, B. Binz, A. Rosch, R. Ritz, P. G. Niklowitz, and P. Böni, *Physical Review Letters* **102**, 186602 (2009), URL <http://link.aps.org/doi/10.1103/PhysRevLett.102.186602>.
- ²⁰ M. Lee, W. Kang, Y. Onose, Y. Tokura, and N. P. Ong, *Physical Review Letters* **102**, 186601 (2009), URL <http://link.aps.org/doi/10.1103/PhysRevLett.102.186601>.
- ²¹ N. Kanazawa, Y. Onose, T. Arima, D. Okuyama, K. Ohoyama, S. Wakimoto, K. Kakurai, S. Ishiwata, and Y. Tokura, *Phys. Rev. Lett.* **106**, 156603 (2011), URL <http://link.aps.org/doi/10.1103/PhysRevLett.106.156603>.
- ²² Y. Li, N. Kanazawa, X. Z. Yu, A. Tsukazaki, M. Kawasaki, M. Ichikawa, X. F. Jin, F. Kagawa, and Y. Tokura, *Physical Review Letters* **110**, 117202 (2013), URL <http://link.aps.org/doi/10.1103/PhysRevLett.110.117202>.
- ²³ H. Watanabe, S. A. Parameswaran, S. Raghu, and A. Vishwanath, *Physical Review B* **90**, 045145 (2014), URL <http://link.aps.org/doi/10.1103/PhysRevB.90.045145>.
- ²⁴ S. X. Huang, F. Chen, J. Kang, J. Zang, G. J. Shu, F. C. Chou, and C. L. Chien, arXiv:1409.7867 [cond-mat] (2014), arXiv: 1409.7867, URL <http://arxiv.org/abs/1409.7867>.
- ²⁵ S. X. Huang, J. Kang, F. Chen, J. Zang, G. J. Shu, F. C. Chou, S. V. Grigoriev, V. A. Dyadkin, and C. L. Chien, arXiv:1409.7869 [cond-mat] (2014), arXiv: 1409.7869, URL <http://arxiv.org/abs/1409.7869>.
- ²⁶ R. Winkler, *Spin-Orbit Coupling Effects in Two-Dimensional Electron and Hole Systems*, Springer Tracts in Modern Physics (Springer, 2003).
- ²⁷ M. S. Dresselhaus, G. Dresselhaus, and A. Jorio, *Group Theory: Application to the Physics of Condensed Matter* (Springer, Berlin, 2010), softcover reprint of hardcover 1st ed. 2008 edition ed., ISBN 9783642069451.
- ²⁸ T. Jeong and W. Pickett, *Physical Review B* **70**, 075114 (2004), URL <http://link.aps.org/doi/10.1103/PhysRevB.70.075114>.
- ²⁹ G. F. Koster, *Space Groups and Their Representations* (Academic Press, 1957), ISBN 9780124337848.
- ³⁰ I. Žutić, J. Fabian, and S. Das Sarma, *Reviews of Modern Physics* **76**, 323 (2004), URL <http://link.aps.org/doi/10.1103/RevModPhys.76.323>.
- ³¹ O. Leonov, arXiv:1406.2177 [cond-mat] (2014), arXiv: 1406.2177, URL <http://arxiv.org/abs/1406.2177>.
- ³² M. A. Ruderman and C. Kittel, *Physical Review* **96**, 99 (1954), URL <http://link.aps.org/doi/10.1103/PhysRev.96.99>.
- ³³ T. Kasuya, *Progress of Theoretical Physics* **16**, 45 (1956), ISSN 0033-068X, 1347-4081, URL <http://ptp.sciencedirect.com/content/16/1/45>.
- ³⁴ K. Yosida, *Physical Review* **106**, 893 (1957), URL <http://link.aps.org/doi/10.1103/PhysRev.106.893>.
- ³⁵ A. Fert, V. Cros, and J. Sampaio, *Nature nanotechnology* **8**, 152 (2013), URL <http://dx.doi.org/10.1038/nnano.2013.29>.
- ³⁶ Y. B. Bazaliy, B. A. Jones, and S.-C. Zhang, *Physical Review B* **57**, R3213 (1998), URL <http://link.aps.org/doi/10.1103/PhysRevB.57.R3213>.
- ³⁷ G. Tatara and H. Kohno, *Physical Review Letters* **92**, 086601 (2004), URL <http://link.aps.org/doi/10.1103/PhysRevLett.92.086601>.
- ³⁸ A. Bauer and C. Pfleiderer, *Physical Review B* **85**, 214418 (2012), URL <http://link.aps.org/doi/10.1103/PhysRevB.85.214418>.
- ³⁹ M. Levy and S. Zhang, *Physical Review Letters* **79**, 5110 (1997), URL <http://link.aps.org/doi/10.1103/PhysRevLett.79.5110>.

Supplementary for “Transport Theory of Metallic B20 Helimagnets”

I. SOLVING BOLTZMANN EQUATION BY PERTURBATION

If the Hamiltonian of the electron depends on the spin, the Kramer degeneracy will be lifted in the presence of a magnetic field. Even the single orbital Hamiltonian contains two different bands. The impurity potential induce not only intraband scattering, but also interband scattering. These scattering are, in general, highly anisotropic and therefore lead to many interesting phenomena. Although the relaxation time approximation, based on the assumption of isotropic system, may still be able to explain experiments qualitatively¹, it is questionable to produce a reliably quantitative description. We have to solve the Boltzmann equation without making any other assumptions. This section will describe a perturbative way to solve this equation. Note that the method presented here is not new, and has already been well explained in the textbook³.

A. Theory

We assume $f(k) = f_0(k) + f_1(k)$, where f_0 is the Fermi distribution function, or the distribution function at equilibrium. The Boltzmann equation can be written as

$$e\mathbf{E} \cdot \mathbf{v}_+(k) \left(\frac{\partial f_0}{\partial \epsilon} \right)_{\epsilon=\epsilon_+(k)} = 2\pi n_i \int \frac{d^3 k'}{(2\pi)^3} \left\{ (f_1^+(k') - f_1^+(k)) T^{++}(k, k') \delta(\epsilon_+(k) - \epsilon_+(k')) + \right. \\ \left. (f_1^-(k') - f_1^+(k)) T^{+-}(k, k') \delta(\epsilon_+(k) - \epsilon_-(k')) \right\} \quad (S1)$$

$$e\mathbf{E} \cdot \mathbf{v}_-(k) \left(\frac{\partial f_0}{\partial \epsilon} \right)_{\epsilon=\epsilon_-(k)} = 2\pi n_i \int \frac{d^3 k'}{(2\pi)^3} \left\{ (f_1^+(k') - f_1^-(k)) T^{-+}(k, k') \delta(\epsilon_-(k) - \epsilon_+(k')) + \right. \\ \left. (f_1^-(k') - f_1^-(k)) T^{--}(k, k') \delta(\epsilon_-(k) - \epsilon_-(k')) \right\}, \quad (S2)$$

where the super(sub)scripts “+/-” refers to the two different bands due to removing Kramer degeneracy in the single electron Hamiltonian. $T^{\sigma, \sigma'}(k, k')$ is the scattering matrix element for electron from the state of $|\sigma, k\rangle$ to the state of $|\sigma', k'\rangle$. Thus, it contains both the intra-band and interband scattering. It is very easy to generalize to the Hamiltonian with more than two bands. Here, we will try the solution in the form of

$$f_1^\pm(k) = g_\pm(k) \left(-\frac{\partial f_0}{\partial \epsilon} \right)_{\epsilon=\epsilon_\pm(k)}.$$

The Boltzmann equation becomes

$$-e\mathbf{E} \cdot \mathbf{v}_+(k) = \frac{n_i}{(2\pi)^2} \int d^3 k' \left\{ (g_+(k') - g_+(k)) T^{++}(k, k') \delta(\epsilon_+(k) - \epsilon_+(k')) + \right. \\ \left. (g_-(k') - g_+(k)) T^{+-}(k, k') \delta(\epsilon_+(k) - \epsilon_-(k')) \right\} \quad (S3)$$

$$-e\mathbf{E} \cdot \mathbf{v}_-(k) = \frac{n_i}{(2\pi)^2} \int d^3 k' \left\{ (g_+(k') - g_-(k)) T^{-+}(k, k') \delta(\epsilon_-(k) - \epsilon_+(k')) + \right. \\ \left. (g_-(k') - g_-(k)) T^{--}(k, k') \delta(\epsilon_-(k) - \epsilon_-(k')) \right\} \quad (S4)$$

$$\mathbf{j} = e \int \frac{d^3 k}{(2\pi)^3} \left(\mathbf{v}_+(k) g_+(k) \left(-\frac{\partial f_0}{\partial \epsilon} \right)_{\epsilon=\epsilon_+(k)} + \mathbf{v}_-(k) g_-(k) \left(-\frac{\partial f_0}{\partial \epsilon} \right)_{\epsilon=\epsilon_-(k)} \right), \quad (S5)$$

where n_i is the density of impurity. To further simplify the notation, we can define the state vector and the linear operator

$$\Phi(k) = \begin{pmatrix} g_+(k) \\ g_-(k) \end{pmatrix} \quad (S6)$$

$$X(k) = -e \begin{pmatrix} \mathbf{E} \cdot \mathbf{v}_+(k) \\ \mathbf{E} \cdot \mathbf{v}_-(k) \end{pmatrix} \quad (S7)$$

$$(W\Phi)_+(k) = \frac{n_i}{(2\pi)^2} \int d^3k' \left\{ (g_+(k') - g_+(k)) T^{++}(k, k') \delta(\epsilon_+(k) - \epsilon_+(k')) + \right. \\ \left. (g_-(k') - g_+(k)) T^{+-}(k, k') \delta(\epsilon_+(k) - \epsilon_-(k')) \right\} \quad (S8)$$

$$(W\Phi)_-(k) = \frac{n_i}{(2\pi)^2} \int d^3k' \left\{ (g_+(k') - g_-(k)) T^{-+}(k, k') \delta(\epsilon_-(k) - \epsilon_+(k')) + \right. \\ \left. (g_-(k') - g_-(k)) T^{--}(k, k') \delta(\epsilon_-(k) - \epsilon_-(k')) \right\} \quad (S9)$$

It is clear that the Boltzmann equation can be written as

$$W\Phi(k) = X(k) . \quad (S10)$$

B. Approximation

We will work at $T = 0$, so that the derivative of Fermi distribution function becomes a delta function. We will integrate over the magnitude of momentum and get the term k^2/v_k . Therefore, it is more convenient to define the “modified” scattering as

$$S_{kk'}^{\sigma\sigma'} = T_{kk'}^{\sigma\sigma'} \left(\frac{k^2}{v_k} \right)_\sigma \left(\frac{k^2}{v_k} \right)_{\sigma'} \quad Z_{\hat{n}}(k) = \begin{pmatrix} v_n^+ \left(\frac{k^2}{v_k} \right)_+ \\ v_n^- \left(\frac{k^2}{v_k} \right)_- \end{pmatrix} .$$

Clearly, in this definition, S is symmetric, ie. $S_{kk'}^{\sigma\sigma'} = S_{k'k}^{\sigma'\sigma}$. In practice, we will expand the wave vector $\Phi(k)$ in terms of spherical harmonic functions. Define the matrix

$$M(k) = \begin{pmatrix} \left(\frac{k^2}{v_k} \right)_+ & 0 \\ 0 & \left(\frac{k^2}{v_k} \right)_- \end{pmatrix} ,$$

and multiply it on both sides of Boltzmann equation.

$$\sum_{\sigma' l' m'} \left(S^{\sigma\sigma'}(l, m; l', m') + (-)^{m+1} \delta_{\sigma\sigma'} \sum_{l_1} \left(\sum_{\sigma_1} S^{\sigma\sigma_1}(l_1, m - m'; 0, 0) \right) B(l_1, m - m'; l', m'; l) \right) g_{\sigma'}(l' m') \\ = Z_{\hat{n}}^\sigma(l, m) \quad (S11)$$

$$g_\sigma(\hat{k}) = \sum_{lm} g_\sigma(l, m) Y_l^m(\hat{k}) , \quad Z_{\hat{n}}^\sigma(\hat{k}) = \sum_{lm} Z_{\hat{n}}^\sigma(l, m) Y_l^m(\hat{k}) \\ S^{\sigma\sigma'}(\hat{k}, \hat{k}') = \sum_{lm} \sum_{l'm'} S^{\sigma\sigma'}(l, m; l', m') Y_l^m(\hat{k}) \left(Y_{l'}^{m'}(\hat{k}') \right)^* \\ B(l_1, m - m'; l', m'; l) = (-)^m \sqrt{(2l_1 + 1)(2l' + 1)(2l + 1)} \begin{pmatrix} l_1 & l' & l \\ m - m' & m' & -m \end{pmatrix} \begin{pmatrix} l_1 & l' & l \\ 0 & 0 & 0 \end{pmatrix} \\ \sigma_n = \frac{1}{(2\pi)^3} \sum_{\sigma l m} (-)^m Z_{\hat{n}}^\sigma(l, m) g_\sigma(l, -m)$$

Note that the Wigner $3j$ symbol is used. Now, it is clear that we can solve the Boltzmann equations in an approximate way.

In practice, we will set a cutoff l_c on the angular momentum of the spherical harmonic functions. Larger l_c produces more precise solutions. In our calculation, we set $l_c = 5$ for limitations on the computing source. We will see that it produces quantitatively different results from the relaxation time approximation.

II. HELICAL RESISTANCE

In this section, we will study the resistance of helical phase in the presence of the spin-orbital coupling. Apply the local $SU(2)$ gauge transformation in Eqn 29, the cubic SOC term becomes

$$\begin{aligned} R^{-1}\sigma_x k_x (k_y^2 - k_z^2)R &= \sigma_x \left(k_x - \frac{2\pi}{d}\sigma_x \right) (k_y^2 - k_z^2) \\ R^{-1}\sigma_y k_y (k_z^2 - k_x^2)R &\approx (\sigma_y \cos \theta - \sigma_z \sin \theta) k_y \left(k_z^2 - \left(k_x - \frac{2\pi}{d}\sigma_x \right)^2 \right) \\ R^{-1}\sigma_y k_z (k_x^2 - k_y^2)R &\approx (\sigma_z \cos \theta + \sigma_y \sin \theta) k_z \left(\left(k_x - \frac{2\pi}{d}\sigma_x \right)^2 - k_y^2 \right) \end{aligned}$$

With the assumption of $1/d \ll k_f$, it is safe to ignore the extra $2\pi/d$ terms in the transformed cubic SOC.

Fig 1 shows the ratio R_{CPW}/R_{CIW} as a function of SOC. It is found that this ratio peaks when SOC vanishes and reaches its minimum when $\alpha = \pi h/(md)$ or $\gamma = 0$. It is argued that the peaks and troughs are related with the anisotropy of the impurity scattering. In this section, we investigate the scattering more systematically, and reveals how the anisotropy of the scattering is changed by SOC.

As in the main text, we consider the case $\beta = 0$ for simplicity. The Hamiltonian is

$$\begin{aligned} H &= H_0 + V \\ H_0 &= \frac{p^2}{2m} - h\sigma_z \\ V &= \gamma\sigma_x p_x + \alpha\sigma_y (p_y \cos \theta + p_z \sin \theta) + \alpha\sigma_z (p_z \cos \theta - p_y \sin \theta) \\ U &= v \mathbf{I}_{2 \times 2} - jh\sigma_z \end{aligned}$$

Here $\gamma = \alpha - \pi/(md)$ and U is the transformed impurity potential. For small SOC $\alpha k_f \ll h$, we treat V as the perturbation and calculate the wavefunction.

$$\begin{aligned} |+, k\rangle &= N_+^{-1}(k_+) \left[\begin{pmatrix} e^{ik_+ r} \\ 0 \end{pmatrix} - \frac{\gamma k_x + i\alpha(k_y \cos \theta + k_z \sin \theta)}{2h} \begin{pmatrix} 0 \\ e^{ik_+ r} \end{pmatrix} \right] \\ |-, k\rangle &= N_-^{-1}(k_+) \left[\begin{pmatrix} 0 \\ e^{ik_- r} \end{pmatrix} + \frac{\gamma k_x - i\alpha(k_y \cos \theta + k_z \sin \theta)}{2h} \begin{pmatrix} e^{ik_+ r} \\ 0 \end{pmatrix} \right] \end{aligned}$$

N_{\pm} are introduced for normalization. In principle, $\theta = 2\pi x/d$ is a space dependent function, and thus will mix the plane wave with different momentum and different fermi surfaces. Here, it is assumed that the space varying is much smaller than the difference of two fermi momentum. Especially, $1/d \ll |k_- - k_+|$, ie. it will not mix two Fermi surfaces. Now, we calculate the scattering matrix elements in the case of strongly spin-dependent impurity potential, eg. $v \approx jh$. After integrating over $\theta(x)$.

$$T^{++}(k, k') = |\langle +k' | U | +k \rangle|^2 \approx \left(\frac{v + jh}{(2h)^2} \right)^2 \left(\gamma^2 k_x k'_x + \frac{\alpha^2}{2} [k_y k'_y + k_z k'_z] \right)^2 \quad (S12)$$

$$T^{--}(k, k') = |\langle -k' | U | -k \rangle|^2 \approx (v + jh)^2$$

$$T^{+-}(k, k') = |\langle -k' | U | +k \rangle|^2 \approx \frac{\gamma^2}{(2h)^2} [(v + jh)k_x - (v - jh)k'_x]^2 + \frac{1}{2} \frac{\alpha^2}{(2h)^2} \left[((v + jh)k_y + (v - jh)k'_y)^2 + (k_y \leftrightarrow k_z) \right]$$

It is easy to see that $T^{++} \ll T^{--}$. The conductivity is dominated by the fermi surface with smaller intraband scattering as those parts with large scattering rate will be “shorted out”². Therefore, we focus only on T^{++} here.

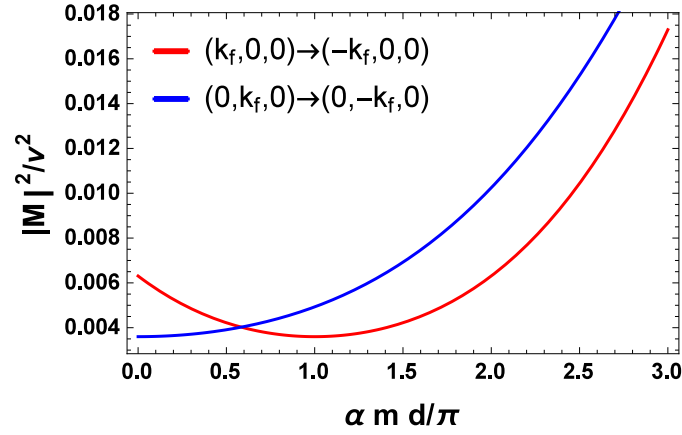


FIG. S1: Scattering magnitude vs. the spin orbital coupling α with $j\hbar/v = 1.06$, and $\beta = 0$. Red: Scattering between $(k_f, 0, 0)$ and $(-k_f, 0, 0)$. It is clear that the scattering rate reaches its minimum when $\alpha \approx \pi/(md)$. This behavior is typical for the scattering between large k_x , which accounts for the resistivity when current is perpendicular to the domain wall. Blue: Scattering between $(0, k_f, 0)$ and $(0, -k_f, 0)$. It monotonically increase with SOC. This is common among the scattering between large k_y (k_z) which accounts for the resistivity when current is parallel to the domain wall.

For currents perpendicular to the domain wall (along \hat{x}), the electrons contributed to this flow are dominated by those with larger k_x since the velocity $v_x \approx k_x/m$. For currents parallel to the domain wall, the electrons contributed to this flow are dominated by those with larger k_y (k_z) since the velocity $v_x \approx k_x/m$ ($v_y \approx k_y/m$). When SOC vanishes $\alpha = 0$, $\gamma \neq 0$, larger k_x and k'_x leads to larger scattering in Eqn S12. Therefore, $R_{CPW} \gg R_{CIW}$, and the ratio reaches its maximum. When $\alpha = \pi/(md)$, $\gamma = 0$, $\alpha \neq 0$, larger k_y and k'_y (or k_z and k'_z) leads to larger scattering. Therefore, $R_{CIW} \gg R_{CPW}$, and the minimum of ratio emerges. When SOC becomes very large, spin on the fermi surface is locked by the direction of the fermi momentum. In this limit, the anisotropy of the scattering vanishes and the ratio approaches to 1, as shown in Fig S1.

* Electronic address: jkang@umn.edu

† Electronic address: jiadongzang@gmail.com

¹ P. M. Levy, and S. Zhang, Phys. Rev. Lett. **79**, 5110 (1997).

² R. Hlubina and T. M. Rice, Phys. Rev. B. **51**, 9253 (1995).

³ Ziman, Electrons and Phonons (Clarendon, Oxford, 1960).